

Towards Understanding Contact Angle Hysteresis Behavior of Textured Surfaces

Marianne J. Case, Ashutosh Shastry, Karl F. Böhringer

University of Washington Engineered Biomaterials (UWEB), Department of Electrical Engineering, University of Washington, Seattle, Washington 98195

ABSTRACT: Bioassay empowered by lab-on-a-chip technologies offers many potential applications and is therefore a worthwhile pursuit. Employing textured surfaces for such droplet-based assay systems is an exciting prospect because of the unique properties of ultrahydrophobic textured surfaces. Hysteresis behavior on these surfaces is therefore an area of keen research. A model of hysteresis as a function

of surface texture could facilitate the surface design process. Potential sources of hysteresis on textured surfaces include pinning due to pillar edges and pinning resulting from contact with pillar top area. Experimental data suggested that contact between the droplet and the surface contributes significantly to hysteresis, whereas pinning of the droplet by pillar edges does not have a significant effect.

1. INTRODUCTION

Interest has grown in lab-on-a-chip technology as a tool useful for analyzing properties of small groups of cells [4,7]. These systems must incorporate a mechanism for shuttling cells to different parts of the chip, such as a droplet-based system in which a water droplet carries one or more cells along the surface of the chip. Several strategies have been employed for moving droplets across surfaces, including electrowetting, surface tension gradients, and temperature gradients [6].

When designing a surface capable of inducing droplet movement, the effects of hysteresis must be considered. Hysteresis, the pinning of the droplet contact line by physical or chemical imperfections [3], acts to reduce droplet movement. Hysteresis of a surface can be quantified by measuring the range of contact angles a droplet can adopt on that surface. On a surface with no imperfections, droplets would maintain an equilibrium contact angle dependent only on the surface tension of the droplet and two phases which it contacts, as given by Young's equation:

$$\cos \theta_E = \frac{\gamma_{SV} - \gamma_{SL}}{\gamma_{LV}}$$

where θ_E is the equilibrium contact angle, S is the solid phase, V is the vapor phase, and L is the liquid (water) phase. While Young's equation holds for droplets on smooth surfaces, it does not apply to droplets on rough surfaces. A droplet may assume one of two configurations on a rough hydrophobic surface. In the Fakir configuration, which occurs on very hydrophobic rough surfaces, the droplet rests on top of the surface projections, trapping air underneath it

within the surface valleys. The contact angle of a droplet in Fakir configuration can be calculated using the Cassie-Baxter relation [1]. Droplets in the Wenzel configuration settle into the texture so that the droplet follows the texture of the surface without allowing air gaps [1]. The contact angle of a droplet in the Wenzel configuration is given by Wenzel's relation [1].

However, blemishes on the surface can pin a droplet edge in one place, preventing the droplet base from expanding or contracting as necessary to assume the equilibrium contact angle. If the droplet's contact angle becomes much different from θ_E , the surface tension imbalance will overcome the pinning effect and the droplet will expand or contract to reestablish a contact angle closer to θ_E .

Thus, the hysteresis of a surface can be quantified using the upper and lower limits of the contact angles that can be assumed on that surface. Equation 2 gives the relation between the contact angle range and contact angle hysteresis [3]: *contact angle hysteresis* $\Delta\theta = \theta_A - \theta_R$ where θ_A is the largest contact angle possible on the surface and θ_R is the smallest angle possible (Fig. 1).

A water droplet resting on a surface with a contact angle gradient ($\theta_2 < \theta_1$) normally experiences a force proportional to the difference in contact angles [2] which moves it towards the area of lower contact angle. However, hysteresis can decrease this force by introducing a range of acceptable contact angles for each side, so that the droplet will not move towards the area of lower contact angle until one of the contact angles has decreased below θ_R or increased above θ_A .

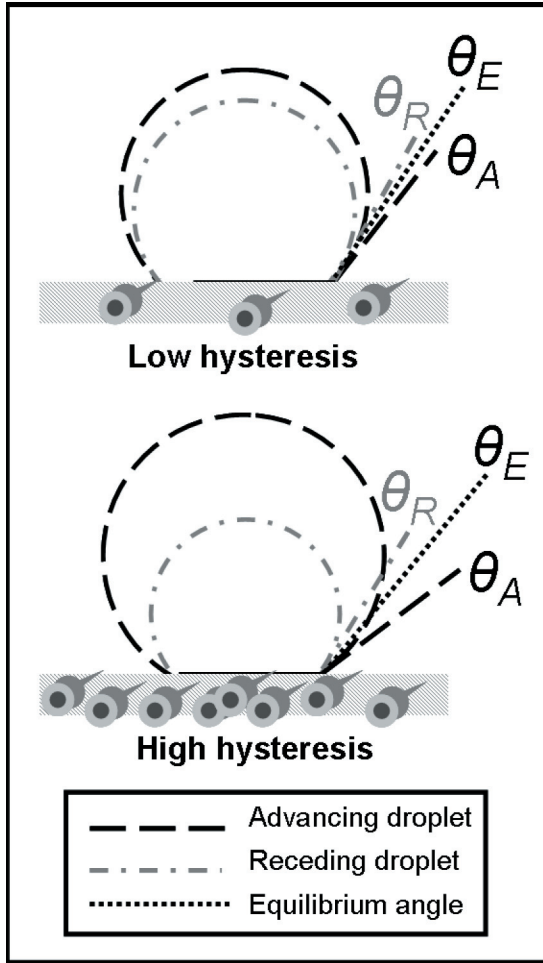


FIGURE 1. CONTACT ANGLE HYSTERESIS

Contact angle hysteresis is low when the difference between θ_A and θ_R is small. A large range between θ_A and θ_R leads to greater contact angle hysteresis.

A contact angle gradient capable of moving a droplet has been created by varying the texture of a surface along its length [5]. However, the force of hysteresis must still be mitigated before the droplet will move. In designing a gradient steep enough to move a droplet without requiring an extra force to mitigate hysteresis, it is necessary to quantify the force of hysteresis with relation to the texture of the surface. This paper will attempt to formulate a mathematical model of the dependence of hysteresis on surface texture and compare the model with experimental measures of hysteresis on textured surfaces.

2. MATERIALS AND METHODS

2.1 Design

Surface roughness can be quantified in term of the roughness parameters, ϕ and r ; where ϕ is the fraction of pillar top area in contact with a droplet divided by total horizontally

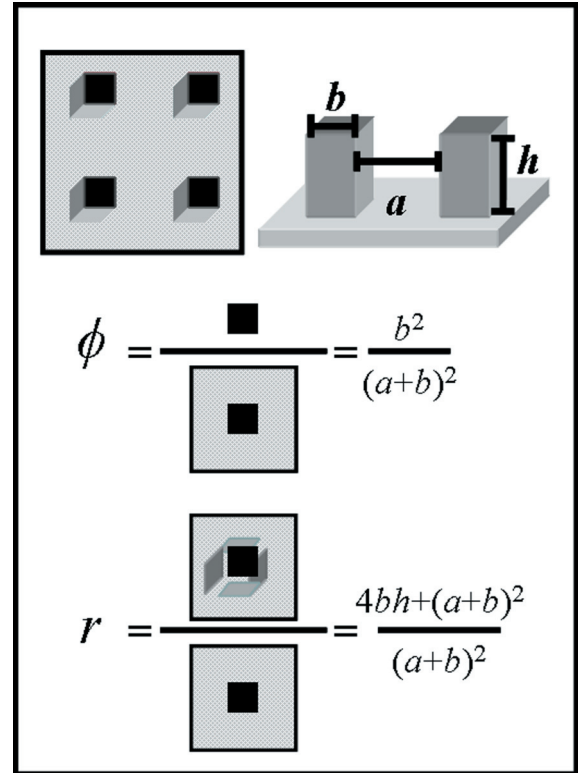


FIGURE 2. TEXTURE AND DESIGN PARAMETERS

The terms ϕ and r are the conventional parameters used to describe the roughness of a surface. The design parameters a , b , and h have been introduced to facilitate the design process.

projected surface area, and r is the fraction of total surface area over horizontally projected surface area [1]. To develop a mathematical model of the relation between ϕ , r , and hysteresis, surfaces with specific combinations of ϕ and r values needed to be created. In order to design these, it became necessary to create three design variables, a (gap length), b (pillar length) and h (pillar height), from which ϕ and r can be calculated. These parameters are shown in Figure 2, along with equations of ϕ and r in terms of a , b , and h .

2.2 Formulation

The model was developed by taking the sources of hysteresis into account. It was assumed that the droplet would experience pinning due to contact with the edges of the pillars. Then the length of pillar edges in contact with the droplet footprint becomes important, and is given by $A_f * b / (b+a)^2$, where R is the radius of the droplet footprint and A_f is the footprint area. The imperfections on the pillar surfaces may also contribute to pinning, necessitating the addition of a second term, $A_f * b^2 / (b+a)^2$. The assumption is made that these terms are both significant and are additive, although experimental data may prove otherwise. The size of the droplet is also expected to affect the level of

hysteresis, with larger droplets contacting more pillars and experiencing greater hysteresis. This leads to Equation 3:

$$\cos(\theta_A - \theta_R) = \left[1 - A_f \left(x \frac{4b}{(b+a)^2} + y \frac{b^2}{(b+a)^2} \right) \right]^n$$

where A_f is the area of the droplet footprint, b is the pillar length, a is the gap length, and x and n are undetermined constants.

2.3 Fabrication

Masks of specific surface textures were created and used in a photolithography process to create wafers that could be etched to form the desired texture and then coated with a hydrophobic material, as shown in Figure 3.

2.4 Characterization

All surfaces tested fit the dimensions required for droplets to assume a Fakir configuration. Each test surface was placed on an FTA200 goniometer produced by First Ten Ångströms (Portsmouth, VA). The goniometer is equipped with a platform which rotates from 0° to 45° and a camera which stays in plane with the platform. Droplets of vary-

ing sizes were positioned in the center of the test surface using a syringe. The platform was tilted until the droplet began to roll.

Care was taken to ensure the tilt motion was slow and constant, so as to avoid any abrupt motion which could send the droplet into a Wenzel configuration. Prior to rotation of the platform, the droplet's left and right contact angles were measured. The average was compared to the contact angles calculated from the Cassie-Baxter equation and from Wenzel's relation [1]. The droplet contact angles θ_A and θ_R just before droplet movement were measured and recorded. The tilt angle of the platform was also recorded.

3. RESULTS

Four surfaces, A-D, were tested. The pillar height h on all surfaces was $88 \mu\text{m}$. The pillar lengths ranged from $45\text{--}100 \mu\text{m}$ and the gap lengths ranged from $25\text{--}40 \mu\text{m}$. The corresponding ϕ values for each surface are given in Figure 4. Surfaces A-C allowed the droplet to roll off when tilted. Surface D appeared to allow droplets to slip into Wenzel regime, causing droplets to stick to the surface even as the platform was rotated up to 45° . Very small droplets also did not roll off the platform. Figure 4 shows the droplets before tilting and just prior to roll-off.

4. DISCUSSION

The tilt angle required to induce roll-off increases as ϕ increases. To study the effect of A_f , two trials were run on surface C using two different drop sizes. Compared to the first trial of surface C, the second trial (shown in Figure 4) required a smaller tilt angle to induce roll-off in a droplet with a slightly smaller footprint. Figure 5 shows that $\cos(\theta_A - \theta_R)$ could be reasonably described by the second term of the model, ϕA_f , suggesting that the x term of the model could be set to zero without introducing significant error. A second degree polynomial fit of the data gave an R^2 value of 0.9072. However, more data and a more rigorous analysis is required to fully evaluate the model.

It is worth noting that the droplets which rolled did so when the advancing contact angle reached 160° . If 160°

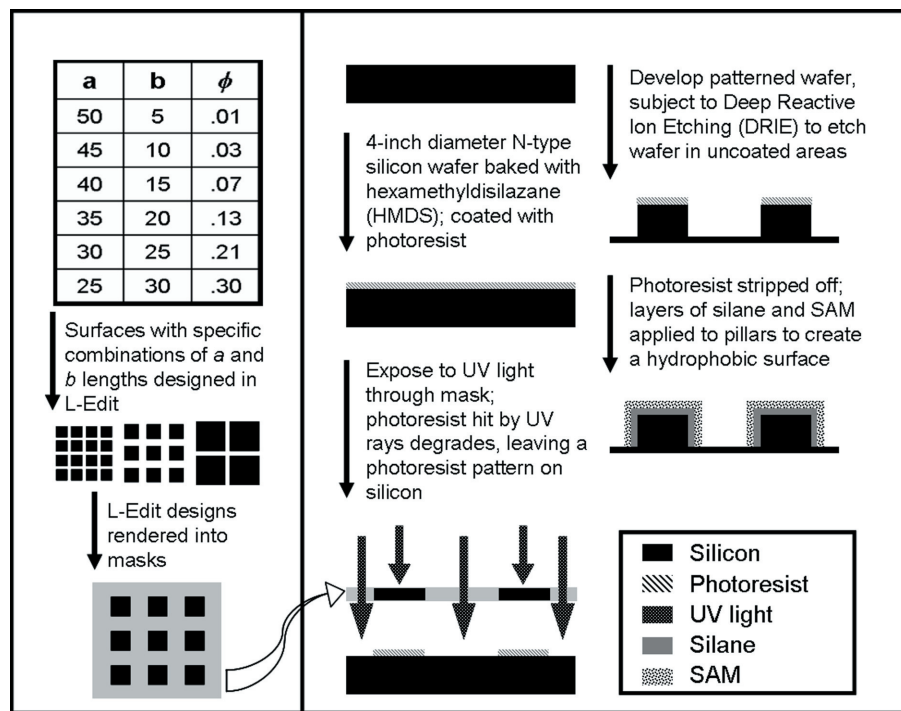


FIGURE 3. CREATING THE SURFACES

(a) Design of the surface: Each design covered an area of 121 mm^2 and appeared twice in the mask. The mask was printed by CAD/Art Services, Inc., in Poway, CA 92064.

(b) Fabrication of the surface: The HMDS bake lasted 30 minutes. The photoresist AZ4620 was applied and a developer solution of AZ400K diluted 1:4 with deionized water was used. The Standard Bosch® process was employed during DRIE to create pillar heights of 88 microns. Tridecafluoro-1,1,2,2-tetrahydrooctyltrichlorosilane (FOTS), which is a self assembling monolayer (SAM), was applied to the surface by Microstructures, Inc. in San Jose, CA 95134.

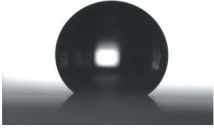
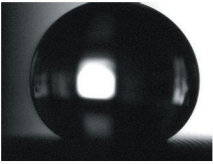
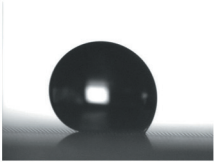
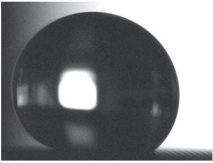
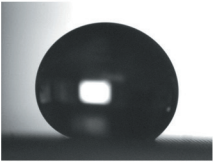
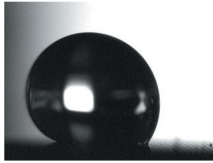
Surface	A	B	C	D
Droplet on level surface				
Contact Angle	(L) 140.22° (R) 139.61°	(L) 146.15° (R) 147.60°	(L) 150.02° (R) 149.68°	to be added
Expected Angle	125.37°	132.66°	136.43°	
Droplet just prior to roll-off				
Contact Angle	(A) 160.53° (R) 123.79°	(A) 160.44° (R) 141.75°	(A) 160.72° (R) 140.06°	to be added
Tilt Angle	38°	17°	9°	45°
ϕ	0.64	0.49	0.42	0.28
Footprint Area	6.18 mm ²	14.07 mm ²	9.58 mm ²	to be added

FIGURE 4. EXPERIMENT RESULTS

Pictures show droplets on the level surface and on the tilted surface just before roll-off, with tilt angles given. The left (L) and right (R) contact angles are listed for the level surfaces. The advancing (A) and receding (R) contact angles are listed for the tilted surfaces. The expected angle is the contact angle the droplet should have assumed in Fakir configuration on the FOTS-coated surface with the given ϕ value, based on the Cassie-Baxter relation. The footprint area is the base area of the droplet just prior to roll-off.

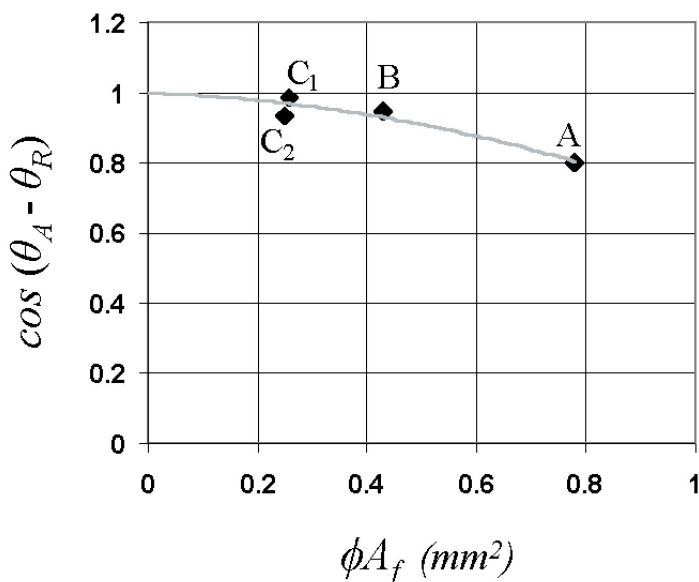


FIGURE 5. PLOT OF SECOND MODEL TERM.

The plot shows a second order relation between the second term of the model and the cosine of the range in contact angles just before roll-off. Two trials of surface C are shown, with the subscripts indicating the trial number. The second trial of C is also represented in Figure 4. Low values of $\cos(\theta_A - \theta_R)$ indicate greater levels of hysteresis. Here, the droplet in \hat{C}_2 appears to experience slightly greater hysteresis compared to \hat{C}_1 , which is inconsistent with its lower A_f value and lower tilt angle.

is the upper limit of the allowed contact angle range, a droplet should move to restore a lower contact angle as soon as the advancing angle exceeds 160°, whether or not the receding angle of the droplet has dropped below the minimum allowed.

The model is limited to droplets in the Fakir configuration. Droplets which had partially or completely slipped into Wenzel configuration could not be induced to roll off the surface, even at the maximum tilt of 45°. While all the surfaces tested were textured so that the Fakir configuration would be more stable than the Wenzel configuration [1], the slight jarring of the droplet which sometimes occurred during platform rotation was sufficient to induce the droplet to adopt a Wenzel configuration. Because the requirements to assure the stability of the Fakir configuration [1] were not stringent enough in this case, and because the measured contact angles at 0° tilt were 12°-14° different than those calculated using the Cassie-Baxter relation, it may be necessary to more thoroughly study the effect of texturing on the water-repelling properties of FOTS-coated surfaces.

5. CONCLUSION

The data qualitatively suggest that the total surface area contacted by the droplet makes a greater contribution to the level of hysteresis experienced by the droplet than does pinning of the droplet due to pillar edges. Departures from expected values in measured contact angle and droplet configuration call for further study of FOTS-coated textured surfaces. More data is necessary to refine and validate the model.

ACKNOWLEDGMENTS

We would like to acknowledge the University of Washington Engineering Biomaterials, a National Science Foundation Engineering Research Center.

REFERENCES

1. Bico J, Thiele U, Quéré D. Wetting of Textured Surfaces. *Colloids and Surfaces* 2002; 206:41–46.
2. Chaudhury M, Daniel S. Rectified motion of liquid drops on gradient surfaces induced by vibration. *Langmuir* 2002;18:3404-3407.
3. de Gennes PG, Brochard-Wyart F, Quéré D. Capillarity and wetting phenomena: Drops, bubbles, pearls, waves. Springer-Verlag, 2004. 300 p.
4. Kricka LJ. Microchips, microarrays, biochips and nanochips: Personal laboratories for the 21st century. *Clinica Chimica Acta* 2001;307:219-223.
5. Shastry A, Case MJ, Böhringer KF. Engineering texture to manipulate droplets in microfluidic systems. *IEEE Conference on Micro Electro Mechanical Systems (MEMS)*, Miami Beach, FL, 2004.
6. Tseng YT, Tseng FG, Chen YF, Chieng CC. Fundamental studies on micro-droplet movement by Marangoni and capillary effects. *Sensors and Actuators A: Physical* 2004;114:292-301.
7. Wang SJ, Saadi W, Lin F, Nguyen C, Jeon NL. Differential effects of EGF gradient profiles on MDA-MB-231 breast cancer cell chemotaxis. *Experimental Cell Research* 2004;300:180-189.